JOURNAL OF COMPUTATIONAL PHYSICS 102, 227–235 (1992)

Elimination of Velocity–Space Rings-and-Spokes Instabilities in Magnetized Electrostatic Particle Simulations of Plasmas

NIELS F. OTANI

School of Electrical Engineering, Cornell University, Ithaca, New York 14853

JIN-SOO KIM[†] AND CHARLES K. BIRDSALL

Electronics Research Laboratory, University of California, Berkeley, California 94720

AND

BRUCE I. COHEN, WILLIAM MCCAY NEVINS, AND NEIL MARON[‡]

Lawrence Livermore National Laboratory, Livermore, California 94550

Received February 23, 1990; revised June 17, 1991

Artificial velocity–space instabilities excited by the discreteness of particles are a nuisance in plasma particle simulations. The suppression of these instabilities is considered for the case of a uniformly magnetized electrostatic particle simulation using a combination of analytical and numerical techniques. It is found that, for a representative "rings-and-spokes" perpendicular velocity distribution modeling a Maxwellian, the instabilities are suppressed if the number of perpendicular velocity "rings" exceeds $\frac{1}{3}(\omega_p/\omega_c)^2$, and the number of gyrophase "spokes" exceeds $8k_{\max}v_{th}/\omega_c$.

I. INTRODUCTION

There are a number of advantages in using particles in computer simulation of plasmas [1]. Among these are the capability of studying kinetic effects in plasmas, plasmas which are far from Maxwellian, plasma sheaths, resonant effects in velocity space, velocity-space instabilities, and wave-breaking following the formation of a shock.

With these advantages come some difficulties. The representation of a plasma as a collection of particles means that noise will in general be present from the particle discreteness. This noise can be much larger than that which is present in a real plasma, because typically no more than a few million particles can be followed by present-day computers, compared to particle counts several orders of magnitude higher in a typical real plasma.

Additionally, the few million particles of a particle simulation can only represent a desired continuous phase space distribution function up to a certain accuracy. Since there are a number of plasma instabilities which are sensitive to the details of the distribution, it is often the case that the particle representation of a desired distribution in a computer model is unstable while the desired distribution itself is not.

These two difficulties are generally dealt with by choosing the particle representation of the desired initial distribution in a judicious manner. There are two philosophies involved in this choice. First, if the particles are initialized or "loaded" in an organized manner, then the noise can be reduced to a minimum [2]. As an extreme example of this philosophy, one could, for example, pick a small number of velocities, chosen so as to model in rough fashion the desired velocity distribution, and then load a large number of particles, uniformly spaced in real space, for each of these velocities. If the number of particles for each velocity is a multiple of the number of simulation grid-points, the charge associated with each velocity will be uniformly distributed to the grid, and there will be no associated noise. In the absence of initial electric or magnetic fields, each of the velocity subpopulations or velocity "beams" will just free-stream, and no noise would ever appear.

Unfortunately, these "multibeam" distributions tend to be unstable [3, 4], even though the corresponding desired velocity distribution may be stable. Any initial perturbation, either user-supplied or from roundoff, will grow to large amplitude. More importantly, the presence of this instability can mask or interfere with the "real" behavior of the distribution. Also, it is generally the case that so many particles are required to uniformly load each beam that only a relatively small number of beams can be used. This results

[†] Present address: Department of Physics, University of California, Irvine, CA 92717.

[‡] Present address: Box 9, Northstar, Alberta, Canada T0H 2T0.

0021-9991/92 $5.00

in only a fair representation of the desired distribution function.

The other philosophy is to load the particles in some random fashion using a probability distribution identical to the desired distribution function. The resulting particle distribution function is a reasonable representation of the desired distribution function and is typically stable in the absence of discernible beams. The resulting simulation is, however, often very noisy.

It is not necessary to employ one of these philosophies to the exclusion of the other. For example, one can load particles in an organized manner which "looks" random. This type of method, often called a "quiet-start" method, has been quite successful. Such a method might, for example, consist of loading particles uniformly in space, but then scrambling the velocities using a bit-reversed choice of velocity indices [5, 6]. This kind of method permits the loading of many different velocities, so that the desired distribution is well represented, while still reducing noise. Another approach is to use beamlike structures, but choose the number of beams, their placement in velocity, and the associated number of particles with both linear stability and noise minimization in mind.

Most of these approaches require something be known about how well each dimension of velocity space should be filled to guarantee linear stability. Work along these lines has been conducted by Gitomer and Adam [3] for the unmagnetized electrostatic case. In this paper, we examine another common and important situation—that of the velocity space perpendicular to a uniform magnetic field in an electrostatic simulation. We address the following questions: How well must perpendicular velocity space be filled to guarantee that no artificial linear instabilities result? How well must gyrophase space be represented?

Our answers to these questions have appeared elsewhere without derivation [7]. In this paper, we present the details of the underlying calculation. The model used in our analysis is described in Section II. We then examine the perpendicular velocity instabilities (ring instabilities) for this model in Section III. The suppression of gyrophase instabilities (spoke instabilities) is considered in Section IV. Some sample simulations are shown in Section V. A summary of results is provided in Section VI.

II. THE MODEL

Our primary interest here is the effect of various perpendicular velocity–space particle distributions on linear stability. For this reason, we will not include finite timestep or spatial grid effects, nor will we consider the effects of particle discreteness in real space. These simplifications allow us to use the continuous forms of the Vlasov equation and Poisson's equation and to take into account the velocity–space particle discreteness simply through the form of the zero-order velocity distribution function. For the plane perpendicular to a static uniform magnetic field in the presence of electrostatic fields, the Vlasov equation is

$$\frac{\partial f}{\partial t}+\mathbf{v}\cdot\nabla_\perp f+\frac{q}{m}\left(\frac{\mathbf{v}\times\mathbf{B}_0}{c}-\nabla_\perp\phi\right)\cdot\frac{\partial f}{\partial \mathbf{v}_\perp}=0, \tag{1}$$

where $f(\mathbf{x}_\perp, \mathbf{v}, t)$ is the distribution function of the species whose discreteness effects we are considering, $\phi(\mathbf{x}_\perp, t)$ is the electrostatic potential, q and m are the (signed) charge and mass of the species, and $\mathbf{B}_0 = B_0\hat{\mathbf{z}}$ is the uniform magnetic field. Note that this equation holds equally well for $\int f\,dv_z$ in place of f, a substitution we make without loss of generality for the remainder of this paper. We shall consider the effect of discreteness in velocity space due to one species only. Poisson's equation is then

$$\nabla^2\phi=-4\pi\left(qn_0\int f\,d\mathbf{v}_\perp+\rho_b\right), \tag{2}$$

with the normalization $\int f\,d\mathbf{v}_\perp = n(\mathbf{x}_\perp, t)/n_0$, where $n(\mathbf{x}_\perp, t)$ and n_0 are the number density and mean number density, respectively. The quantity $\rho_b \equiv -qn_0$ represents a fixed, neutralizing background charge. Only one species is employed in our calculations. We expect that the other species making up the background charge, if represented as particles, would display properties qualitatively similar to those described here, and further, by their presence, would not qualitatively affect the properties discussed here.

We take our zero-order distribution function to be of the form $f_0(v_\perp, \theta-\Omega t)$, which is uniform in space and independent of the time t, apart from a trivial contribution from cyclotron gyro-rotation in velocity space. Here $\theta \equiv -\tan^{-1} v_y/v_x$ is the gyrophase and $\Omega \equiv qB_0/mc$ is the particle species cyclotron frequency. In what follows, we shall be considering linear perturbations about equilibrium systems characterized by zero-order distribution functions of this type. In particular, we will be making much use of "multi-ring" and "rings-and-spokes" distributions. Use of these distributions simplifies the analysis and leads to principles and properties which we can expect are applicable to more general distributions.

III. RING INSTABILITIES

We first consider a zero-order gyrophase-independent distribution function of the form

$$f_0(v_\perp)=\frac{1}{2\pi v_\perp}\sum_{s=1}^{N} a_s\delta(v_\perp-v_{\perp s}), \tag{3}$$

where the a_s's and $v_{\perp s}$'s are constants with $\sum_s a_s = 1$, and we defer consideration of the discreteness of the distribution function in gyrophase to the next section. The dispersion relation for the case of a uniformly magnetized uniform plasma in the electrostatic approximation is well known when the zero-order distribution depends only on $v_\perp$ [8]. For the N-velocity-ring distribution Eq. (3), we obtain the dispersion relation

$$0 = D(k, \omega) \equiv 1 - \sum_{s=1}^{N} \frac{2}{kr_s} \frac{\omega_{ps}^2}{\Omega^2} \times \sum_{l=1}^{\infty} J_l(kr_s)[J_{l-1}(kr_s) - J_{l+1}(kr_s)] \times \frac{l^2\Omega^2}{\omega^2 - l^2\Omega^2}, \tag{4}$$

where k is the perpendicular wavenumber, ω is the wave frequency, $\omega_{ps}^2 \equiv 4\pi q^2 a_s n_0/m$ is the plasma frequency, $r_s \equiv v_{\perp s}/\Omega$ is the gyroradius corresponding to the sth velocity ring, and the J_l's are Bessel functions of the first kind of order l. The modes resulting from this dispersion relation bear a similarity to Dory–Guest–Harris modes [9], which occur for a single, finite-temperature velocity ring.

A simple root-finder was devised to determine the roots to Eq. (4). The root-finder uses the Newton–Raphson method on the dispersion relation (4) and its derivative with respect to ω^2. No attempt is made to follow roots as k is incremented; instead, guesses are made for each value of k. These guesses are spaced two per each interval of $[n\Omega, (n+1)\Omega]$ in the pattern,

$$\omega = \cdots, (n+\varepsilon)\Omega, (n+1-\varepsilon)\Omega, (n+1+\varepsilon)\Omega, (n+2-\varepsilon)\Omega, \ldots, \tag{5}$$

where n is an integer and ε is a parameter chosen much less than one. This method is employed because of the existence of poles in Eq. (4) at $\omega = n\Omega$. The algorithm has been very successful, not only in plotting real roots versus k, but also in determining thresholds for the onset of instability. The latter is characterized by the meeting and subsequent disappearance of two roots as k is varied; see Fig. 1.

We examined the stability of a distribution which employed "equally weighted rings" i.e., rings with equal values of a_s with values of $v_{\perp s}$ as shown in Fig. 2a. The values of $v_{\perp s}$ are obtained from the condition

$$\frac{s}{N+1} = \frac{\int_0^{v_{\perp s}} e^{-v_\perp^2/2v_{th}^2} v_\perp \, dv_\perp}{\int_0^{\infty} e^{-v_\perp^2/2v_{th}^2} v_\perp \, dv_\perp}, \quad s = 1, \ldots, N,$$

while, of course, $a_s = 1/N$ for all s. Note that this definition automatically determines the $v_{\perp \max} \equiv v_{\perp N}$. For $N = 32$,

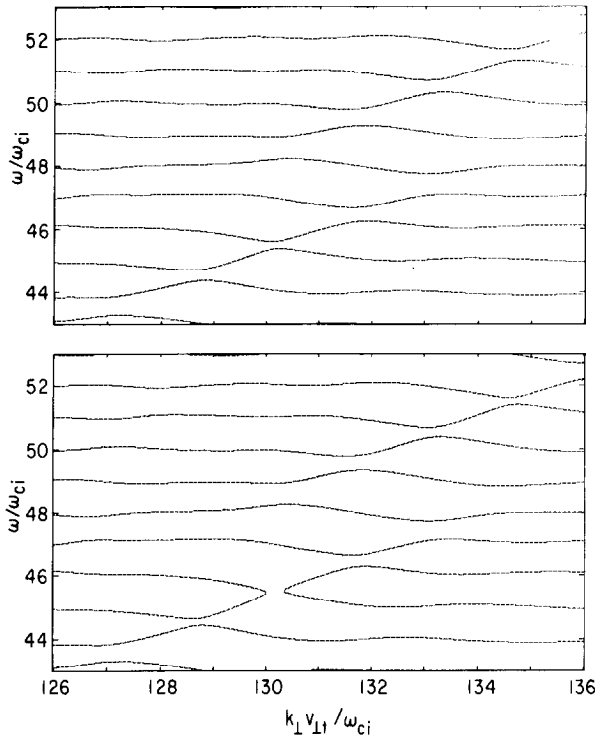

FIG. 1. Typical root-solver-generated dispersion diagrams: (a) shows the solver's capability at large values of ω and k, for $\omega_{pi}^2/\Omega_i^2 = 220$; (b) shows the onset of instability when ω_{pi}^2/Ω_i^2 is increased to 240.

$v_{\perp \max} = 2.64 v_{th}$; for $N = 64$, $v_{\perp \max} = 2.89 v_{th}$. Another possibility, that of equally spaced rings (in $v_\perp$), is defined by the assignment $v_{\perp s} = s v_{\perp \max}/N$, where now $v_{\perp \max}$ may be freely chosen. The weights would then be defined according to

$$a_s = v_{\perp s} e^{-v_{\perp s}^2/2v_{th}^2} \Big/ \sum_{s'=1}^{N} v_{\perp s'} e^{-v_{\perp s'}^2/2v_{th}^2},$$

as shown in Fig. 2b. The equally spaced rings case was not studied here.

Unstable roots for a fixed value of N, the number of velocity rings, were found by increasing the value of $\omega_p^2/\Omega^2 \equiv \sum_s \omega_{ps}^2/\Omega^2$ until the phenomenon illustrated in Fig. 1, characteristic of the onset of instability, was observed somewhere in ω-k space. Plots covering large regions of ω-k space were made first to obtain an estimate of the critical value of ω_p^2/Ω^2. Then, regions where the characteristic behavior was observed were analyzed more carefully, using small increments in the value of ω_p^2/Ω^2, in order to obtain a more accurate determination of the critical value.

Perhaps the most significant result of this search is shown in Fig. 3. We find that a velocity distribution with a given value of ω_p^2/Ω^2 is stable if the number of (equally weighted) rings representing the distribution, N, exceeds $\frac{1}{3}(\omega_p^2/\Omega^2)$.

We also find that, as ω_p/Ω is increased for fixed N, the

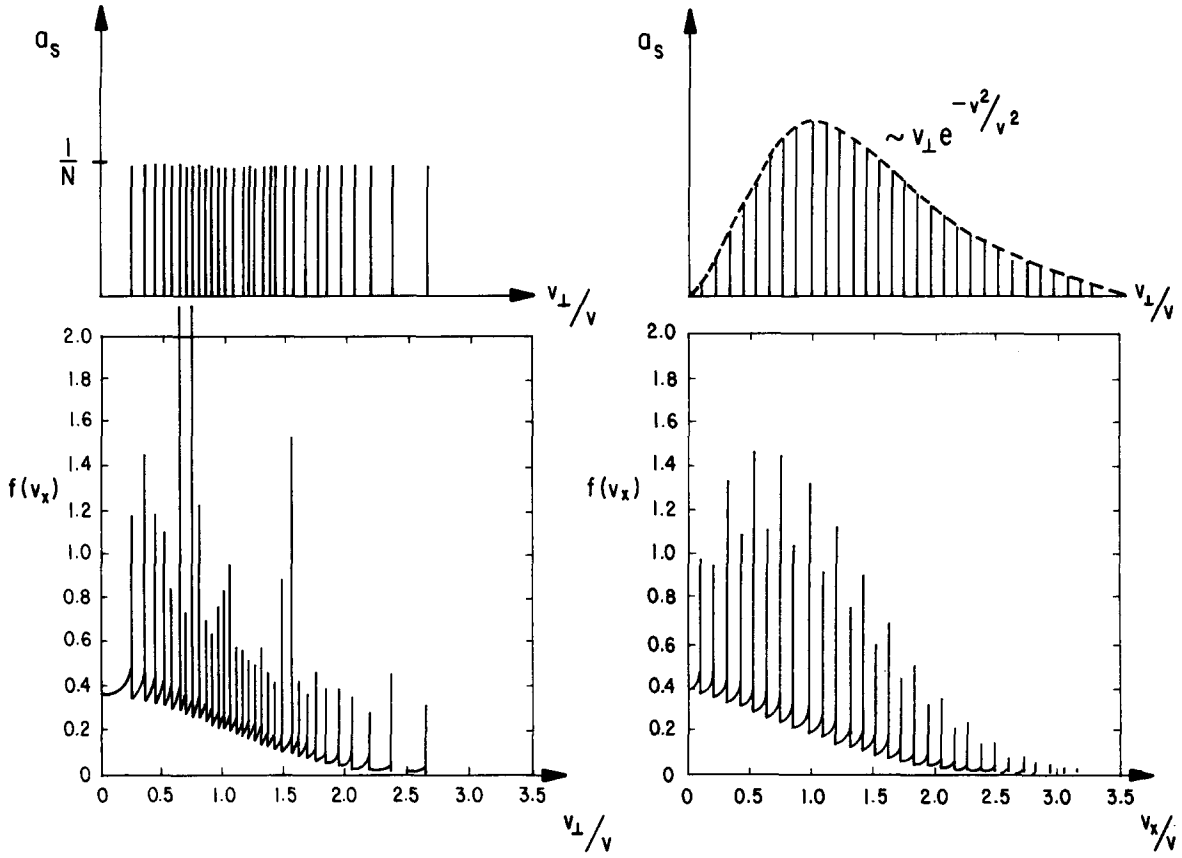

FIG. 2. Weights, a_s, and projected velocity distributions $f(v_x)$ for a velocity ring representation of a Maxwellian velocity distribution in $v_\perp$ for (a) equally weighted, unequally spaced rings in perpendicular velocity space, and (b) unequally weighted, equally spaced rings.

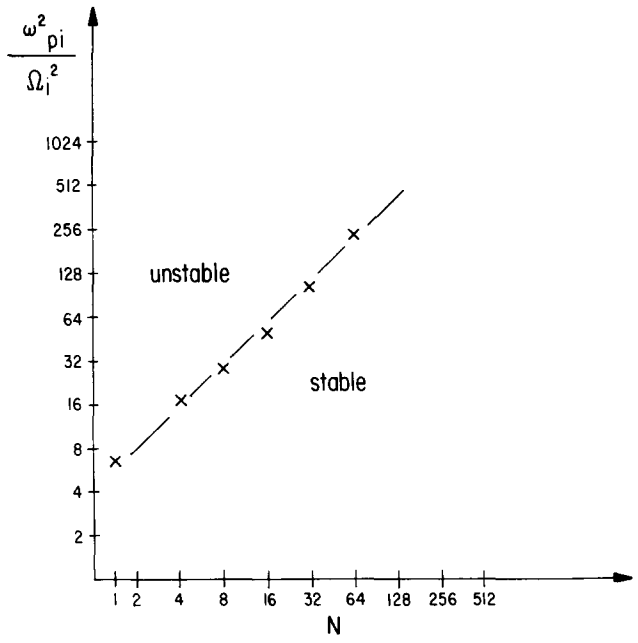

FIG. 3. The ω_p^2/Ω^2 stability boundary vs. N for Maxwellian-representative distributions containing N equally weighted rings.

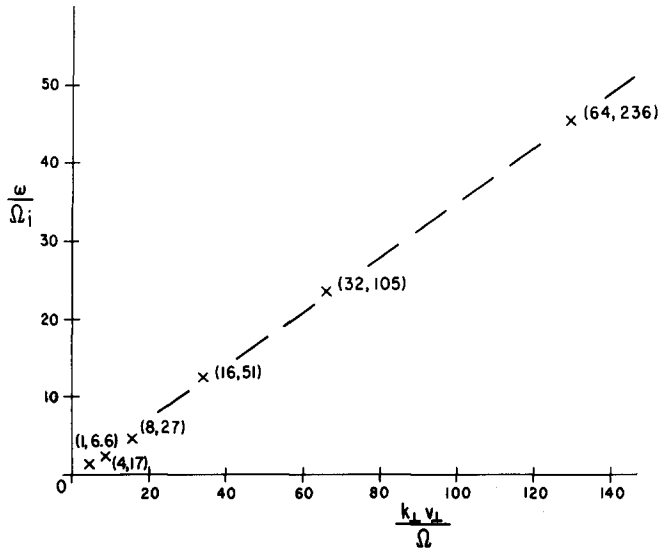

FIG. 4. The distribution composed of N equally weighted rings first becomes unstable at the values of ω and $k_\perp$ shown labeled by $(N, \omega_p^2/\Omega^2)$, where the value of ω_p^2/Ω^2 is stability threshold displayed in Fig. 3.

first mode to go unstable is characterized by increasingly large values of k and ω, as illustrated in Fig. 4. We observe that the critical value of k roughly satisfies $kv_\perp/\Omega \approx 2N$ while, approximately, $\omega/\Omega \approx 3N/4$.

Thus, we can expect that, without considering other factors, if the number of velocity rings is chosen a safe margin above $\frac{1}{3}(\omega_p^2/\Omega^2)$, the resulting distribution will have stability properties acceptable for the purposes of particle simulation. The short wavelength and high frequency associated with the most unstable mode for large N may in fact allow some relaxation in this stability criterion; after all, the simulation will not be able to follow frequencies higher than $\pi/\Delta t$ or wavenumbers larger than $\pi/\Delta x$, Δt and Δx being the timestep and grid spacing, respectively. Some evidence for this less stringent stability criterion has in fact been seen in simulations [10]. Definitive statements to this effect require an examination of alias and resonance effects associated with the grid and finite timestep [11], and thus are beyond the scope of the present study.

IV. SPOKE INSTABILITIES

We now consider how the above results are modified due to the particle discreteness in gyrophase space. Two derivations were performed for this purpose leading to the same dispersion relation. We present here the simpler of these two derivations, using results from the more involved derivation only to motivate our initial assumptions. The simpler derivation is based on a method employing action-angle variables as described in Aamodt *et al.* [12]. The single-particle Hamiltonian for a monochromatic electrostatic plane wave takes the form [12, 13]

$$\begin{aligned} H &= H_0 + H_1 \\ &= \mu\Omega + q\phi_1/m \\ &= \mu\Omega + (q/m)\, e^{ikx} \sum_r \bar{\phi}_r e^{ir\Omega t - i\omega t} \\ &= \mu\Omega + (q/m)\, e^{ikX} \sum_l J_l(kr_g)\, e^{il\theta} \\ &\quad \times \sum_r \bar{\phi}_r e^{i(r\Omega - \omega)t}, \end{aligned} \tag{6}$$

where $r_g \equiv v_\perp/\Omega$ is the gyroradius and μ, θ, X, and Y are the canonical set of variables expressible in terms of the usual Cartesian phase space coordinates as

$$\mu \equiv \frac{v_x^2 + v_y^2}{2\Omega} = \frac{v_\perp^2}{2\Omega}, \tag{7}$$

$$\theta = -\arctan\frac{v_y}{v_x}, \tag{8}$$

$$X \equiv x + \frac{v_y}{\Omega}, \tag{9}$$

$$Y \equiv y - \frac{v_x}{\Omega}, \tag{10}$$

with the ambiguity in sign in Eq. (8) determined by $v_x = v_\perp \cos\theta$, $v_y = -v_\perp \sin\theta$. The wave is assumed to be propagating in the $\mathbf{k}_\perp \equiv k\hat{\mathbf{x}}$ direction, which has been taken parallel to $\hat{\mathbf{x}}$ without loss of generality.

The form of the mode perturbation expressed in Eq. (6) indicates that the harmonics of the cycloron frequency will be coupled. A parallel, but more complicated derivation, described briefly in Appendix *A*, provides additional insight. The coupling occurs in the first place because the zero-order distribution function now depends on θ and thus loses the symmetry in gyrophase assumed in the previous section. The coupling is, however, limited to frequencies which are integer multiples of the cyclotron frequency away, by the persistence of symmetry with respect to translation in time by the cyclotron period $2\pi/\Omega$, i.e., $f_0(\mu, \theta, t) = f_0(\mu, \theta, t + 2\pi/\Omega)$. The validity of the assumption is also supported a posteriori from the consistency of the derived dispersion relation.

Canonical transformation of Eq. (6) to the new variables $(\bar{\theta}, \bar{\mu})$ using the generating function $F_2 = (\theta - \Omega t)\bar{\mu}$ yields $\bar{\theta} = \partial F_2/\partial\bar{\mu} = \theta - \Omega t$, $\mu = \bar{\mu} = \partial F_2/\partial\theta$, and

$$\begin{aligned} \bar{H} &= H + \partial F_2/\partial t = q\phi/m = \bar{H}_1 \\ &= (q/m)\, e^{ikX} \sum_l J_l(kr_g)\, e^{il\theta} \\ &\quad \times \sum_r \bar{\phi}_r \exp\{i[(r+l)\,\Omega - \omega]t\}. \end{aligned} \tag{11}$$

Note the explicit time dependence of $\bar{\theta}$ on t. The equilibria we are considering are thus of the form $f_0 = f_0(\mu, \bar{\theta})$. These are valid equilibria since both μ and $\bar{\theta}$ are constants of the unperturbed motion. In fact, to zero order in the perturbation $q\phi/m$, all of the independent variables are dynamical invariants:

$$\frac{d}{dt}(\bar{\theta}, \bar{\mu}, X, Y)^{(0)} = 0. \tag{12}$$

In particular, $\bar{\theta}$ is the gyrophase measured relative to a co-rotating reference angle and, hence, is constant along an equilibrium trajectory.

The Vlasov equation may be written in terms of the Hamiltonian H as

$$f(t) - f(0) = \int_{-\infty}^{t} dt' \{H, f\}, \tag{13}$$

where $\{\ \}$ is the Poisson bracket. When linearized with respect to H_1/H_0, in the new canonical coordinates, this equation becomes

$$f_1 = \int_{-\infty}^{t} dt' \left(\frac{\partial \bar{H}_1}{\partial \bar{\theta}} \frac{\partial f_0}{\partial \mu} - \frac{\partial \bar{H}_1}{\partial \mu} \frac{\partial f_0}{\partial \bar{\theta}} \right). \tag{14}$$

When Eq. (11) is substituted, Eq. (14) yields

$$\begin{aligned} f_1 &= \sum_{r'} \bar{f}_{1r'} e^{ikx} \exp[-i(\omega - r'\Omega)t] \\ &= -\frac{q}{m} \sum_r \bar{\phi}_r \\ &\quad \times \sum_l \frac{lJ_l(\partial f_0/\partial \mu) + i(\partial J_l/\partial \mu)(\partial f_0/\partial \bar{\theta})}{\omega - (r+l)\Omega} \\ &\quad \times \exp\{ikX + il\bar{\theta} + i[(r+l)\Omega - \omega]t\}. \end{aligned} \tag{15}$$

Use of Poisson's equation $-\nabla^2\phi = 4\pi q n_0 \int \Omega\ d\mu\, d\bar{\theta} f_1$ enables us to obtain a dispersion relation

$$\begin{aligned} k^2 \bar{\phi}_r = \omega_p^2 \sum_{l,l'} \int \Omega\, d\mu\, d\bar{\theta} f_0 \\ \times \frac{lJ_l(\partial J_{l'}/\partial \mu) + l' J_{l'}(\partial J_l/\partial \mu)}{\omega - (r+l')\Omega} \\ \times e^{i(l-l')\bar{\theta}} \bar{\phi}_{r-(l-l')}. \end{aligned} \tag{16}$$

The determinant of the implied (infinite) matrix, Hermitian when ω is real, serves as the dispersion function for the general case $f_0 = f_0(\mu, \bar{\theta})$. Generalization of Eq. (16) to more species is straightforward, requiring simply that the right-hand side be summed over species. As expected, the eigenmodes for this system do not in general have the simple time dependence $e^{-i\omega t}$, but instead are composed of a mixture of frequencies Ω apart. This is a consequence of the time-dependent equilibrium $f_0(\mu, \theta, t)$ and expresses the coupling between modes that is consistent with the corresponding assumption in Eq. (6). As a check, we find that the well-known gyrophase-independent dispersion relation

$$1 + \frac{\omega_p^2}{k^2} \int 2\pi\Omega\, d\mu \frac{\partial f_0}{\partial \mu} \sum_l \frac{lJ_l^2(kr_g)}{\omega - l\Omega} = 0 \tag{17}$$

is recovered when $\partial f_0/\partial \bar{\theta} = 0$. Also, Eq. (16) is found to be consistent with the reality condition $\phi_r^*(k, \omega) = \phi_{-r}(-k, -\omega^*)$.

We now choose the equilibrium distribution function as

$$f_0 = M^{-1} \sum_{m=1}^{M} \delta(\bar{\theta} - \theta_m) f_0(\mu). \tag{18}$$

This distribution function may be said to be composed of M angular "spokes" and is thus the "rings-and-spokes" distribution shown in Fig. 5 when $f_0(\mu)$ is given by the sum of Dirac delta functions $f_0(\mu) = \Omega^{-1} \sum_s a_s \delta(\mu - \mu_s)$. If the angles θ_m are evenly spaced, $\theta_m = 2\pi m/M$, then

$$M^{-1} \sum_m \exp[i(l-l')\theta_m] = \delta_{l', l+jM}, \tag{19}$$

where $\delta_{l',l}$ is the Kronecker delta and $j = 0, \pm 1, \pm 2, \ldots$. Hence,

$$\begin{aligned} \bar{\phi}_r = \frac{\omega_p^2}{k^2} \sum_{l,j} \int \Omega\, d\mu f_0(\mu) \\ \times \frac{l\partial(J_l J_{l+jM})/\partial \mu + jMJ_{l+jM}(\partial J_l/\partial \mu)}{\omega - (r+l+jM)\Omega} \\ \times \bar{\phi}_{r+jM}. \end{aligned} \tag{20}$$

The presence of M evenly-spaced spokes shortens the temporal period of repetition to $2\pi/M\Omega$, accounting for the alias coupling of modes separated in frequency by $M\Omega$ rather than Ω.

The Bessel functions in Eq. (20) have the small-argument limiting form $J_l(kr) \sim (kr/2)^l/l!$ and $|J_l(kr)| \ll 1$ for $|kr| < l/2$. Thus, only terms such that $|jM| \leqslant 2k(r_g)_{\max}$ contribute in Eq. (20), since $J_l(kr_g)$ goes to zero very rapidly once $|l|$ is appreciably larger than kr_g. In particular, if $M \geqslant 2k(r_g)_{\max}$, decoupling of the various temporal modes occurs so that only the diagonal terms (i.e., those terms coupling ϕ_r to itself) in Eq. (20) contribute, and the gyrophase-independent dispersion relations Eqs. (4) and (17) are then recovered. In other words, the rings-and-spokes distribution behaves essentially like the corresponding gyrophase-independent distribution when the wavelength is longer than the spacing of M particles arranged on a circle of radius $(r_g)_{\max}$.

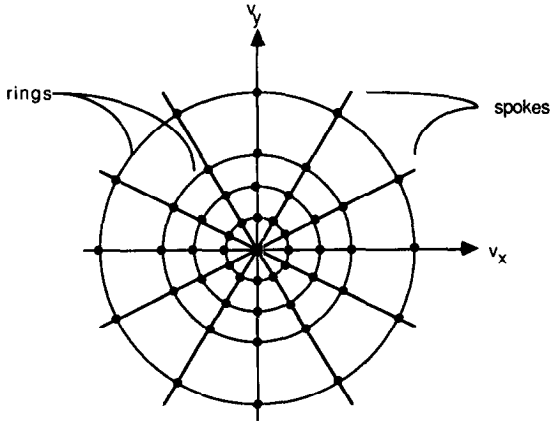

FIG. 5. Location of particles in perpendicular velocity space in a rings-and-spokes distribution. Particles are situated at the intersections of circles concentric about $v_\perp = 0$ (rings) and uniformly spaced lines extending radially from $v_\perp = 0$ (spokes).

In a typical simulation with a thermal velocity distribution, $\max(v_\perp) < 4v_{th}$. Hence, the argument of the Bessel functions in Eq. (20) satisfies the inequality $kr_g < 4k_{\max} v_{th}/\Omega$. The coupling of $\tilde{\phi}_r$ to $\tilde{\phi}_{r+jM}$ will be negligible, with some margin of safety, if

$$M > 8k_{\max} v_{th}/\Omega. \tag{21}$$

The analysis of Section III may then be applied. For N equally weighted rings, stability can be achieved for

$$N > \frac{1}{3}\left(\frac{\omega_p}{\Omega}\right)^2. \tag{22}$$

Thus, a quiet-start simulation ought to be *stable* to magnetized multi-ring instabilities if the inequalities in Eqs. (21) and (22) are both satisfied.

V. SIMULATION STUDY

A small number of simulation runs were performed to test our theory. Rings-and-spokes distributions representative of a Maxwellian (and therefore physically stable) plasma were employed. In these runs, the distribution function was replicated eight times across the length of the system to quiet the first few spatial modes. The first simulation, shown in Fig. 6, employed the parameters $\omega_p^2/\Omega^2 = 200$ and $N = 299$ which, according to the analysis of Section III, is stable to ring instabilities. However, with the thermal velocity chosen such that $8k_{\max} v_{th}/\Omega = 50$, i.e., greater than the number of spokes, $M = 32$, we find that the velocities in the tail of the distribution $2.5v_{th} \leqslant v_\perp \leqslant 3v_{th}$ give arguments falling near the maxima of J_l for $14 \leqslant |l| \leqslant 18$. Diagnostic analysis of the simulation revealed the signature of the cyclotron alias coupling as lower hybrid normal modes near $\mathrm{Re}(\omega) = \pm 14\Omega$ coupled to modes at $\mathrm{Re}(\omega) = \pm(14-32)\Omega = \pm 18\Omega$; these modes all grew with rate $\mathrm{Im}(\omega) = 0.15\Omega$, with the ratios of the coupling modes being equal as expected, $|\phi(k, 14\Omega)|^2/|\phi(k, -18\Omega)|^2 = |\phi(k, -14\Omega)|^2/|\phi(k, 18\Omega)|^2$.

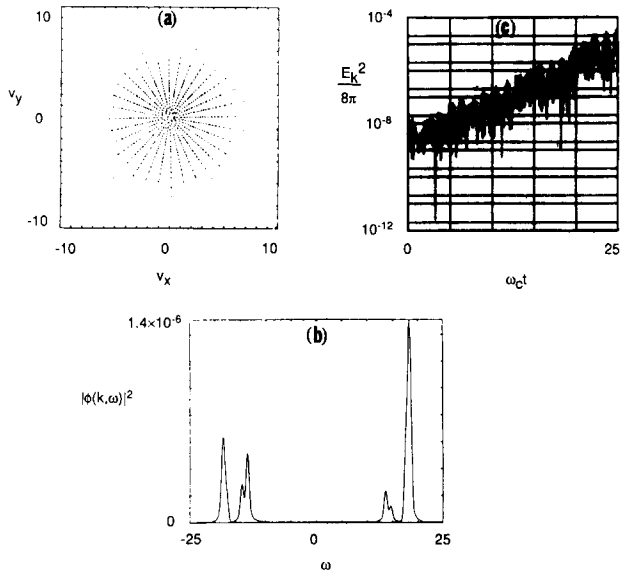

FIG. 6. Simulation of a Maxwellian plasma with a separable rings-and-spokes perpendicular velocity distribution function for electrostatic flute modes $\mathbf{k} \cdot \mathbf{B}_0 = 0$. The parameters were $\omega_p^2/\Omega^2 = 200$, $N = 299$, and $M = 32$ for six operable values of k: $kv_{th}/\Omega = 1.25, 2.50, 3.75, 5.00$, and 6.25: (a) Perpendicular velocity distribution function. Apparent structure at low velocities is due to the particular sampling of 3000 particles out the 76,544 total. (b) Power spectrum $|\phi(k, \omega)|^2$ as a function of the frequency ω. (c) The corresponding field energy $E^2(k)/8\pi$, integrated over ω as a function of time Ωt for $kv_{th}/\Omega = 6.25$.

We next doubled M to $M = 64$, so that both Eqs. (21) and (22) were satisfied. Figure 7 shows that modes near the lower hybrid frequencies $\mathrm{Re}(\omega) = \pm 14\Omega$ were excited and may have been very weakly unstable. However, if there was instability, saturation occurred very quickly and at a very small amplitude $E_1^2/8\pi n_0 T = 10^{-11}$, which was not much above the initial amplitude. In fact, the fluctuation level in the normal modes was so small that the discrete particle

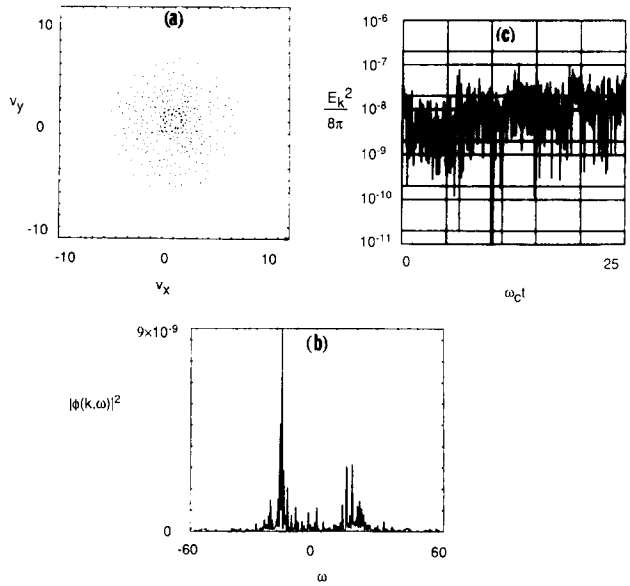

FIG. 7. Effectively stable rings-and-spokes simulation with the same plasma parameters as in Fig. 6 and with $N = 149$, $M = 64$, and 76,288 total particles: (a) Sampling of perpendicular velocity distribution function. (b) Power spectrum $|\phi(k, \omega)|^2$ as a function of frequency ω. (c) $E^2(k)/8\pi$ as a function of time Ωt for $kv_{th}/\Omega = 6.25$.

ballistic noise was visible in the power spectrum (Fig. 7b). For our purposes, this simulation corresponded to a stable quiet start.

VI. SUMMARY

A root solver has been used to determine how many rings, equally weighted in perpendicular velocity space, are required for the stability of a distribution representative of a Maxwellian distribution in an electrostatic, uniformly magnetized particle simulation. We find that the number of rings should exceed $\frac{1}{3}(\omega_p/\Omega)^2$ for stability. This determination assumes that the rings were of uniform density in gyrophase space.

It was next determined analytically how many particles, uniformly distributed in gyrophase space, are required to produce a velocity ring distribution which behaves as a collection of rings of uniform gyrophase density. Dispersion functions for the general distribution $f_0(\mu, \bar{\theta})$, the discrete-particle distribution, and the rings-and-spokes distribution were derived and found to be consistent with well-known gyrophase-independent dispersion relations. We find that the eigenmodes are, in general, not simple sinusoidal functions of time but, instead, are a mixture of frequencies. However, in the case of a Maxwellian rings-and-spokes distribution, we find that the different frequencies decouple when the number of particles per ring (i.e., number of spokes) is larger than $8k_{\max}v_{th}/\Omega$, in which case the dispersion relation reduces to its gyrophase-independent counterpart. These results have been supported by simulations.

The conclusion to be drawn is thus simple. In an electrostatic particle simulation which is uniformly magnetized perpendicular to the simulation plane, if the number of rings exceeds $\frac{1}{3}(\omega_p/\Omega)^2$ and the number of spokes in each ring exceeds $8k_{\max}v_{th}/\Omega$ in a rings-and-spokes representation of a Maxwellian perpendicular velocity distribution, velocity–space stability is guaranteed. These criteria should also serve as reasonable guidelines if the distribution to be used is either not of the rings-and-spokes variety, or is not Maxwellian. If, in addition, the usual precautions are taken with regard to finite timestep and grid effects, it should be possible to perform quiet-start simulations that are stable to artificial magnetized velocity–space instabilities. Such guidelines have in fact been followed with success, as, for example, in research conducted by Cohen, Maron, and Smith [13].

APPENDIX A: ALTERNATIVE DERIVATION

The dispersion relations presented in Section IV may also be derived without the use of Hamiltonian theory. The calculation is more complicated, but perhaps more physical, since expressions for f_1, $\mathbf{E}_1$, ϕ, and ρ_1 are obtained and used explicitly as intermediate results. A summary of this derivation follows.

From the linearized Vlasov equation,

$$\frac{\partial f_1}{\partial t}+\frac{q}{m\Omega}\mathbf{v}_\perp\cdot\mathbf{E}_{1\perp}\frac{\partial f_0}{\partial \mu} + \frac{q}{m\Omega}\mathbf{E}_1\times\mathbf{v}_\perp\cdot\hat{\mathbf{z}}\frac{1}{2\mu}\frac{\partial f_0}{\partial\bar{\theta}}=0, \tag{A1}$$

we obtain

$$f_1(\mathbf{z},\omega)=\frac{qr_g}{2im\omega}\left[e^{i\theta}E_1^+(\mathbf{z},\omega+\Omega)\left(\frac{\partial f_0}{\partial\mu}+\frac{i}{2\mu}\frac{\partial f_0}{\partial\bar{\theta}}\right) + e^{-i\theta}E_1^-(\mathbf{z},\omega-\Omega)\left(\frac{\partial f_0}{\partial\mu}-\frac{i}{2\mu}\frac{\partial f_0}{\partial\bar{\theta}}\right)\right], \tag{A2}$$

where $\mathbf{E}_1=-\nabla\phi$, $E_1^\pm=E_{1x}\pm iE_{1y}$, and, for brevity, $\mathbf{z}\equiv(\mu,\bar{\theta},X,Y)$. The perturbed electric field may be expressed as a function of the zero-order invariants $\mathbf{z}$ as

$$\mathbf{E}_1(\mathbf{z},\omega)=-\int\frac{d^2k_\perp}{(2\pi)^2}e^{i\mathbf{k}_\perp\cdot\mathbf{X}} \times\sum_l J_l(k_\perp r_g)\,e^{il(\bar{\theta}+\alpha)} \times i\mathbf{k}_\perp\phi(\mathbf{k}_\perp,\omega+l\Omega), \tag{A3}$$

where $\mathbf{X}\equiv(X,Y)$, $k_x\equiv|\mathbf{k}_\perp|\cos\alpha$, and $k_y\equiv|\mathbf{k}_\perp|\sin\alpha$. The perturbed charge density may be expressed in terms of f_1 as

$$\rho_1(\mathbf{k}_\perp,\omega)=qn_0\int dt\,e^{i\omega t} \times\int d\mathbf{z}\,e^{-i\mathbf{k}_\perp\cdot\mathbf{x}_\perp(\mathbf{z},t)}f_1(\mathbf{z},t). \tag{A4}$$

where $d\mathbf{z}\equiv\Omega\,dX\,dY\,d\mu\,d\bar{\theta}$, $\mathbf{x}_\perp(\mathbf{z},t)$ and $\mathbf{v}_\perp(\mathbf{z},t)$ are the Cartesian spatial and velocity coordinates as functions of $\mathbf{z}$ and t, and $f_1(\mathbf{z},t)\equiv f_1(\mathbf{x}_\perp(\mathbf{z},t),\mathbf{v}_\perp(\mathbf{z},t),t)$. When this expression is combined with Poisson's equation, we obtain

$$\phi(\mathbf{k}_\perp,\omega)=\frac{4\pi qn_0}{k_\perp^2}\int d\mathbf{z}\,e^{-i\mathbf{k}_\perp\cdot\mathbf{X}} \times\sum_l J_l(k_\perp r_g)\,e^{-il(\bar{\theta}+\alpha)} \times f_1(\mathbf{z},\omega-l\Omega). \tag{A5}$$

Each of Eqs. (A2), (A3), and (A5) involves the coupling of frequencies which are multiples of the cyclotron frequency apart, consistent with the Hamiltonian given in Eq. (6).

When Eqs. (A2) and (A3) are substituted into Eq. (A5) with $\mathbf{k}_\perp = k\hat{\mathbf{x}}$, the result is Eq. (16). The derivation of these equations as summarized above thus serves as a second derivation, confirming the results of the calculation presented in Section IV.

ACKNOWLEDGMENTS

We are grateful to M. Gerver and K. P. Kenyon for a number of illuminating discussions. Research was performed under the auspicies of Department of Energy Contract Nos. DE-AT03-76ET53064 and W-7405-ENG-48, and Cornell University.

REFERENCES

1. See, for example, C. K. Birdsall and A. B. Langdon, *Plasma Physics via Computer Simulation* (McGraw-Hill, New York, 1985); R. W. Hockney and J. W. Eastwood, *Computer Simulation Using Particles* (Adam Hilger, Bristol, 1988); and J. M. Dawson, *Rev. Mod. Phys.* **55**, 403 (1983), and references therein.
2. J. A. Byers, in *Proceedings, Fourth Conference on Numerical Simulation of Plasmas*, edited by J. P. Boris and R. Shanny (U.S. Government Printing Office, Washington, DC, 1970), p. 496; J. A. Byers and M. Grewal, *Phys. Fluids* **13**, 1819 (1970).
3. S. J. Gitomer and J. C. Adam, *Phys. Fluids* **19**, 719 (1976).
4. J. M. Dawson, *Phys. Rev.* **118**, 381 (1960).
5. J. M. Hammersley and D. C. Handscomb, *Monte Carlo Methods* (Methuen, London, 1964).
6. C. K. Birdsall and A. B. Langdon, *Plasma Physics via Computer Simulation* (McGraw-Hill, New York, 1985), p. 393.
7. Ref. [6, pp. 400–402].
8. S. Ichimaru, *Basic Principles of Plasma Physics, A Statistical Approach* (Benjamin, Reading, Mass., 1973), Section 3.4C.
9. R. A. Dory, G. E. Guest, and E. G. Harris, *Phys. Rev. Lett.* **14**, 131 (1965).
10. K. P. Kenyon, M. S. Thesis, University of California, Berkeley, 1984; ERL Memo UCB/ERL M84/64, July 27, 1984, U. C. Berkeley.
11. See Ref. [6, p. 196ff].
12. R. E. Aamodt, B. I. Cohen, Y. C. Lee, C. S. Liu, D. R. Nicholson, and M. N. Rosenbluth, *Phys. Fluids* **24**, 55 (1981).
13. B. I. Cohen, N. Maron, and G. R. Smith, *Phys. Fluids* **25**, 821 (1982).